Applied Surface Science 393 (2017) 37–45

Contents lists available at ScienceDirect

Applied Surface Science

journal homepage: www.elsevier.com/locate/apsusc

Full length article

Controllable growth of polyaniline nanowire arrays on hierarchical macro/mesoporous graphene foams for high-performance flexible supercapacitors

Pingping Yu[a,b], Xin Zhao[a,*], Yingzhi Li[a], Qinghua Zhang[a,*]

[a] State Key Laboratory for Modification of Chemical Fibers and Polymer Materials, College of Materials Science and Engineering, Donghua University, Shanghai 201620, China
[b] Department of Materials Science, Fudan University, Shanghai 200433, China

ARTICLE INFO

Article history:
Received 6 July 2016
Received in revised form
23 September 2016
Accepted 23 September 2016
Available online 24 September 2016

Keywords:
Hierarchical porous structure
Graphene foam
Polyaniline
Supercapacitors
Flexible

ABSTRACT

Free-standing hierarchical macro/mesoporous flexible graphene foam have been constructed by rational intergration ofwell dispersed graphene oxide sheets and amino-modified polystyrene (PS) spheres through a facile "*templating and embossing*" technique. The three dimensional (3D) macro/mesoporous flexible graphene foam not only inherits the uniform porous structures of graphene foam, but also contains hierarchical macro/mesopores on the struts by sacrificing PS spheres and the activation of KOH, which could providing rapid pathways for ionic and electronic transport to high specific capacitance. Vertically polyaniline (PANI) nanowire arrays are then uniformly deposited onto the hierarchical macro/mesoporous graphene foam(fRGO-F/PANI) by a simple *in situ* polymerization, which show a high specific capacitance of 939 F g^{-1}. Thanks to the synergistic function of 3D bicontinuous hierarchical porous structure of graphene foam and effective immobilization of PANI nanowires on the struts, the assembled symmetric supercapctior with fRGO-F/PANI as electrodes exhibits a maximum energy density and power density of 20.9 Wh kg^{-1} and 103.2 kW kg^{-1}, respectively. Moreover, it also displays an excellent cyclic stability with a 88.7% retention after 5000 cycles.

1. Introduction

Supercapacitors (SC) with a high power capability and relatively large energy density compared to conventional capacitors have attracted considerable attention and will be a promising candidate for energy storages [1]. Recently, great efforts have been dedicated to develop porous graphene materials, including crumpled graphene [2,3], holey graphene sheets and graphene foam [4,5], as free-standing electrodes for high-performance flexible supercapacitors. Compared to original graphene sheets, porous graphene structure has a larger surface area which can increase the contact interfaces of electrode/electrolyte and also facilitate the ion diffusions [6]. Moreover, three-dimensional (3D) porous frameworks could provide multi-dimensional pathways for efficient ionic and electronic transport, resulting in a good electrochemical performance.

Among the porous graphene materials, graphene foam (GF) has attracted lots of attentions due to its partly inheriting the properties of two dimensional graphene into 3D macroporous structure and the freestanding and flexible features. Its macroporous structure brings about light-weight, excellent conductivity and adsorption characteristics [7–9]. However, the free-standing GF suffers from lacking of well-defined interconnected hierarchical mesopores or micropores, which exhibits relatively low energy density because of the less efficiency of mass transport and charge storage for supercapacitor. To address the inferior energy densities of GF, the hierarchical structure combined materials with different functions would be a promising approach to provide on both power and energy densities. Wu et al. integrated mesoporous silica walls within 3D interconnected macroporous graphene-based frameworks, showing high specific capacitance and good rate capability [10]. Choi et al. demonstrated a 3D macroporous graphene film (e-CMG) prepared using polystyrene (PS) colloidal particles as sacrificial template, and then a thin layer of MnO_2 was additionally deposited onto e-CMG, which delivered a 2-fold higher specific capacitance than that of e-CMG [11]. Liu et al. also synthesized the nitrogen-doped 3D graphene frameworks by the similar method as anode for lithium-ion batteries [12]. Wang et al. fabricated a N and S doped hierarchically porous graphene (DHPG) electrode through a facile *in situ* constructing strategy in nickel foam using

* Corresponding authors.
E-mail addresses: xzhao@dhu.edu.cn (X. Zhao), qhzhang@dhu.edu.cn (Q. Zhang).

http://dx.doi.org/10.1016/j.apsusc.2016.09.119
0169-4332/

graphene oxide (GO), sulfonated polystyrene (S-PS) spheres, and poly(vinyl pyrrolidone) (PVP) as precursors. The novel electrodes exhibit ultrafast charge/discharge rate capabilities due to the synergistic effects of the well-defined structure and heteroatom doping [13]. Therefore, it is highly attractive to build up hierarchical porous architectures of 3D graphene network by integrating small channels within interconnected macroporous frameworks.

Polyaniline (PANI) has become a good candidate for supercapacitor electrodes due to its low cost, easy synthesis and high pseudocapacitance [14–16]. PANI nanowires with highly-ordered are beneficial to facilitate ion transport by shorten diffusion pathways [17–19]. While the considerable volume changes and mechanical degradation during the repeated intercalation and depletion of ions in the charge/discharge process are the bottleneck for its practical application [20]. Wang et al. synthesized PANI nanowire arrays on flexible PS macrosphere/reduced graphene film with 3D hierarchical structure by the following removal of PS templates, which exhibited high specific capacitance of 740 F g^{-1} [21]. Chen et al. reported that nanostructured PS-PANI/reduced graphene oxide hybrid composites as supercapacitor electrodes showed a specific capacitance of 180 F g^{-1} at a current density of 0.5 A g^{-1} [22,23]. Therefore, 3D free-standing hierarchical porous structure graphene foam can act as robust supporting materials to improve the cycle stability and specific capacitance of PANI.

In our previous work, a novel porous reduced graphene oxide foam (RGO-F)/PANI nanowires composite was fabricated by *in situ* polymerization, showing a high specific capacitance (790 F g^{-1} at a current density of 1 A g^{-1}) as flexible supercapacitor [24]. However, the free-standing RGO-F exhibits low specific surface area and lacks of well-defined interconnected mesopores/micropores, leading to relatively low energy density. Therefore, the incorporation of meso-/micropores into the RGO-F/PANI composites can enhance the specific capacitance and energy density. Herein, we employed a "*templating and embossing*" technique to fabricate a free-standing, light-weight and hierarchical macro/mesoporous flexible foam (fRGO-F) by using PS colloidal particles as sacrificial templates accompanying with the activation of KOH. Nickel foams (NF) were immersed in the GO and amino-modified PS mixed suspension, and fRGO-F was obtained by the removal of NF and following calcination in N_2 atmosphere, as shown in Fig. 1. The PS particles could be served as effective "*spacers*" to effectively avoid the aggregation of reduced GO sheets. The unique hierarchical structures could not only boost ion and electron movements in electrochemical processes but also enabled the porous fRGO-F to serve as a 3D skeleton to combine with pseudoactive materials such as vertically aligned polyaniline (PANI) nanowires with a high mass loading. Controllable growth of PANI nanowire arrays on the fRGO-F networks can enhance the specific capacitance and ensure the utilization of the porous frameworks of the flexible substrate. The fRGO-F/PANI flexible composite could well retain the interconnected framework of fRGO-F, which facilitates easy access of the electrolyte ions to the electrodes. The symmetric SC device based on fRGO-F/PANI electrodes in the 1 M H_2SO_4 electrolyte exhibits a specific capacitance of 939 F g^{-1}, a maximum power density and energy density of 20.9 Wh kg^{-1} and 103.2 kW kg^{-1}, respectively. Besides, it also displays a good cycling performance of 88.7% of the initial capacitance over 5000 cycles.

2. Experimental sections

2.1. Synthesis of hierarchical macroporous fRGO-F

GO was prepared by a modified Hummers method, the details have been described elsewhere [25]. In a typical process, amine group functional PS spheres (0.2 g) were added into the GO suspension (5 mg mL^{-1}) under the magnetic stirring and sonication for 2 h (denoted as fGO). In order to obtain the rational ratio of PS to GO, the fGO films were prepared through brief vacuum filtration. The porosity of fGO films can be controlled by the initial mass loading of PS spheres and the samples are designated as fGOx% (x is the mass loading of PS). The SEM images of fGO10% (Fig. S1A and B) show the PS spheres were uniformly sandwiched between the GO sheets. However, the fGO20% film (Fig. S1C and D) suffered from the collapsing and fracturing as increasing the amount of PS spheres. Therefore, NF sheet (2 cm × 2 cm, 0.1 cm thick, 1 Ω cm^{-2}, from Shenzhen Luchuang Environmental Audio Supplies limited Company) washed by dilute HCl solution and was immersed into the fGO solution for 1 h and then dried in an oven at 60 °C. This step was repeated for several times to ensure that the GO sheets sandwiched with PS spheres fully wrap on the struts of NF. Then the NF templates were etched by 3 M HCl at 60 °C for 5 h and the prepared foam washed with deionized water several times. After being soaked in KOH solution, the precursor was calcinated in N_2 at 1000 °C for 1 h. Then the obtained product fRGO-F was washed with acetic acid, deionized water and ethanol, with a weight of 0.61–0.65 mg cm^{-2}. Besides, parallel sample RGO-F was also fabricated by the same procedure without PS spheres and KOH.

2.2. Preparation of fRGO-F/PANI

The fRGO-F were immersed into the aqueous solution of aniline monomers in 1 M H_2SO_4 (40 mL) without stirring for 3 h. Ammonium persulfate (APS) in 40 mL 1 M H_2SO_4 as an oxidizing agent was rapidly added in the above and stirred for 1 min. The molar ratio of aniline to APS was controlled to be 4:1. After reacting at −5 °C for 12 h, the green layer could be observed on the 3D fRGO-F network. Then the fRGO-F/PANI hybrids were washed with deionized water repeatedly, and dried at 60 °C for 24 h. The composites of fRGO-F/PANI5 and fRGO-F/PANI7 were prepared with the aniline concentration of 0.05 M and 0.07 M, respectively. The mass loading of PANI nanowires in fRGO-F/PANI5 and fRGO-F/PANI7 composites was 0.80 ± 0.05 and 1.56 ± 0.05 mg cm^{-2}, respectively, which was calculated by the weight difference before and after polymerization. Each electrode was tested three times to eradicate any discrepancies.

2.3. Structural and morphological characterization

The morphology and microstructure of the samples were investigated by FESEM (HitachiS-8000) and TEM (JEM-2100). The Raman spectra were obtained by a Raman spectrometer (Renishaw micro-Raman spectroscopy) with He–Ne laser excitation at 632.8 nm and scanning for 50 s. X-ray photoelectron spectroscopy (XPS) was performed on a PHI 5000C ESCA System using a monochromatic Al X-ray source (97.9 W, 1486.6 eV). Data analysis was carried out using RBD AugerScan 3.21 software provided by RBD Enterprises. BET surface area and pore size were conducted by nitrogen adsorption-desorption method at 77 K (Micromeritics Tristar ASAP 3000).

2.4. Electrochemical performances

All the supercapacitor performance was studied on a CHI 660D electrochemical workstation (CH Instruments, Inc., China). Cyclic voltammetry (CV), electrochemical impedance spectroscopy (EIS), and galvanostatic charge/discharge measurements were carried out in a two-electrode system. The fRGO-F, fRGO-F/PANI5 and fRGO-F/PANI7 electrodes and separator were wetted in 1 M H_2SO_4 aqueous electrolyte overnight. Two pieces of the obtained fRGO-F or fRGO-F/PANI composite electrodes were assembled together with a cellulose paper as separator and two Ti wires as

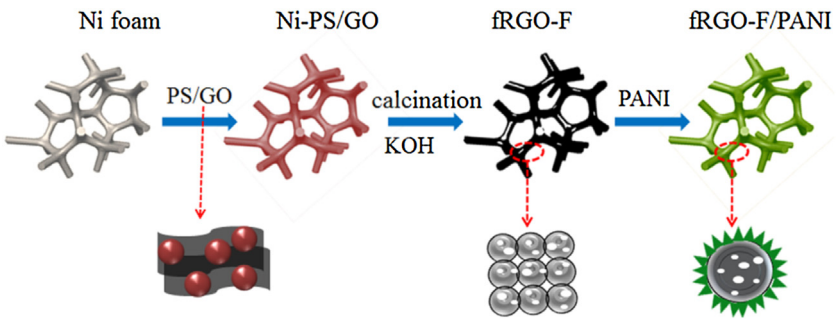

Fig. 1. Scheme illustration of the fabrication procedures of the fRGO-F/PANI.

conductors, and then the total device was encapsulated by a flexible poly (ethylene terephthalate) film.

In a symmetric device, the specific capacitance (C_{sc}) of the electrodes (RGO-F, RGO-F/PANI composites) was obtained by the equation: $C_{sc} = 4I \cdot t/m \cdot V$, where I(A) is the discharge current, t (s) is the discharge time, m (g) is the total mass of two active electrodes, and V (V) is the discharge voltage range. The volumetric capacitance (C_{vol}) of the electrodes was calculated from the equation of $C_{vol} = C_{sc} \cdot r$, where r (g cm^{-3}) is the packing density of the electrode. The energy density (E) and power density (P) of the symmetric supercapacitors were obtained by the equation: $E = C_{sc} \cdot V_{max}{}^2/8$ and $P = V_{max}{}^2/(4m \cdot R_{ESR})$. The equivalent series resistance (R_{ESR}) is estimated by $R_{ESR} = V_{drop}/(2I)$, where V_{drop} (V) is the voltage drop at the beginning of the discharge and I (A) is the constant current.

3. Results and discussion

3.1. Microstructure and morphology

The free-standing of RGO-F obtained by a facile "*templating and embossing*" technique shows the 3D hierarchical porous network structure (Fig. 2A) with a high flexibility. The well-defined porous foam also shows a high electrical conductivity (1204 S m^{-1}). It is noteworthy that the positive charged PS spheres are assembled with negative charged GO sheets by electrostatic interactions, resulting in the uniformly distribution of PS spheres as "*spacers*" between the GO sheets. The high magnification SEM image (Fig. 2B) of fRGO-F struts exhibits opened hierarchical macroporous structure with the pore size of about 1 μm, indicating carbonized PS spheres wrapped by graphene sheets. The good "*sheet contact*" between graphene and carbon spheres gives a good mechanical property and electrical conductivity of fRGO-F. The modified PS spheres could be fully wrapped by the thin GO sheet (Fig. S2), and GO sheets exhibit unfolded and crumple transparent morphology. Compared with the fGO, the fRGO-F shows an interconnected porous structure after etching the PS templates (Fig. 2C). The interfaces between carbonized PS spheres are connected together to form graphene walls in the assembled 3D structure, which is good to prevent the porous structure from collapsing. With KOH as activating agent, the mesopores (10–50 nm) are clearly observed in the graphene walls as shown in Fig. 2D. This hierarchical porous framework can promote fast transmission of the electrons and decrease the transport path of the electrolyte in the high rate process.

Fig. 3A shows the PANI nanowires of fRGO-F/PANI5 was uniformly coated on the graphene spheres, demonstrating a diameter of 20 nm and a length of 100 nm (Fig. 3B). Fig. 3C shows that the length and the distribution density of PANI nanowires increase at the concentration of aniline of 0.07 M. Note that there are vertically PANI nanowires deposited on the internal face of graphene spheres as shown in Fig. 3D, providing a large mass loading of PANI. The tuneable PANI nanowires can be controlled by the concentration of aniline monomer. Protonated aniline monomers are preferred to absorb on the surface of nitrogen-doped fRGO-F due to the π-πinteractions during polymerization process [26]. TEM image of fRGO-F/PANI7 in Fig. 3E identifies the hierarchical porous structure of calcination graphene spheres. In the high magnification TEM image (Fig. 3F), the PANI nanowire arrays with a diameter of 20–50 nm and the length of 100 nm was uniformly coated on the graphene sheets. Apparently, the "*V-type*" PANI nanowires are vertically deposited on both internal and external surfaces of porous graphene sheets.

The porosity of fRGO-F/PANI composites were also tested by N_2 adsorption instrument, and the adsorption isotherms for fRGO-F and fRGO-F/PANI are shown in Fig. 4A. All samples are the typical IV isotherm curves implying the existence of macro-mesoporous structure. The pores are formed by the interconnected graphene spheres and ordered PANI nanowires. The surface areas are calculated based on the Brunauer–Emmett–Teller (BET) theory. The specific surface area decreases from 80 m^2 g^{-1} for fRGO-F to 64 m^2 g^{-1} for fRGO-F/PANI5 and to 70 m^2 g^{-1} for fRGO-F/PANI7. The decrease in the specific surface area with increase of the PANI loading is mainly due to the pore-filling of PANI, which is proved by the changes of average pore sizes and the pore size distributions as shown in the inset of Fig. 4A. The pore size distribution reveals that fRGO-F/PANI possesses macropores and mesopores with a diameter of 10–100 nm, which is consistent with the morphologies of fRGO-F/PANI in Fig. 3.

The Raman spectra of fGO, fRGO-F and fRGO-F/PANI composites are shown in Fig. 4B. D and G bands are observed at ~1317 cm^{-1} and ~1573 cm^{-1}, respectively. The G band corresponds to the first-order scattering of the E_{2g} mode from the sp^2 carbon domains and the D band originates from the defects of the sp^2 domains [27]. The intensity ratio of D and G bands (I_D/I_G) can evaluate the quality of the graphitic structures. Therefore, the value of I_D/I_G of fRGO-F is 1.10, which is lower than that of fGO (1.67), indicating the increase of graphitic carbon in fRGO-F after the calcinations process at a high temperature. Compared to that fGO and fRGO-F, several characteristic peaks can be observed for fRGO-F/PANI, indicating that PANI nanowires have been successfully deposited on the fRGO-F network. The peaks at 1160 cm^{-1} and 1243 cm^{-1} can be assigned to the C—H bending of quinoid ring and C—H bending of the benzenoid ring, respectively. The vibration of semiquinone radical, C=C stretching of the quinoid and C—C stretching of the benzenoid ring are around 1332 cm^{-1}, 1495 cm^{-1} and 1586 cm^{-1}, respectively [28].

X-ray photoelectron spectroscopy (XPS) was further performed to characterize the composition of the samples, and the typical spectra for fRGO-F and fRGO-F/PANI are shown in Fig. 4C. The fRGO-F/PANI sample shows a pronounced N 1 s peak, whereas only a weak N signal is detected on fRGO-F sample. The N atoms in fRGO-F are calculated from XPS analysis is 0.7 at%, which might be derived from the amine group on PS and the N_2 atmosphere during the calcination process. The N 1s peak in fRGO-F has three

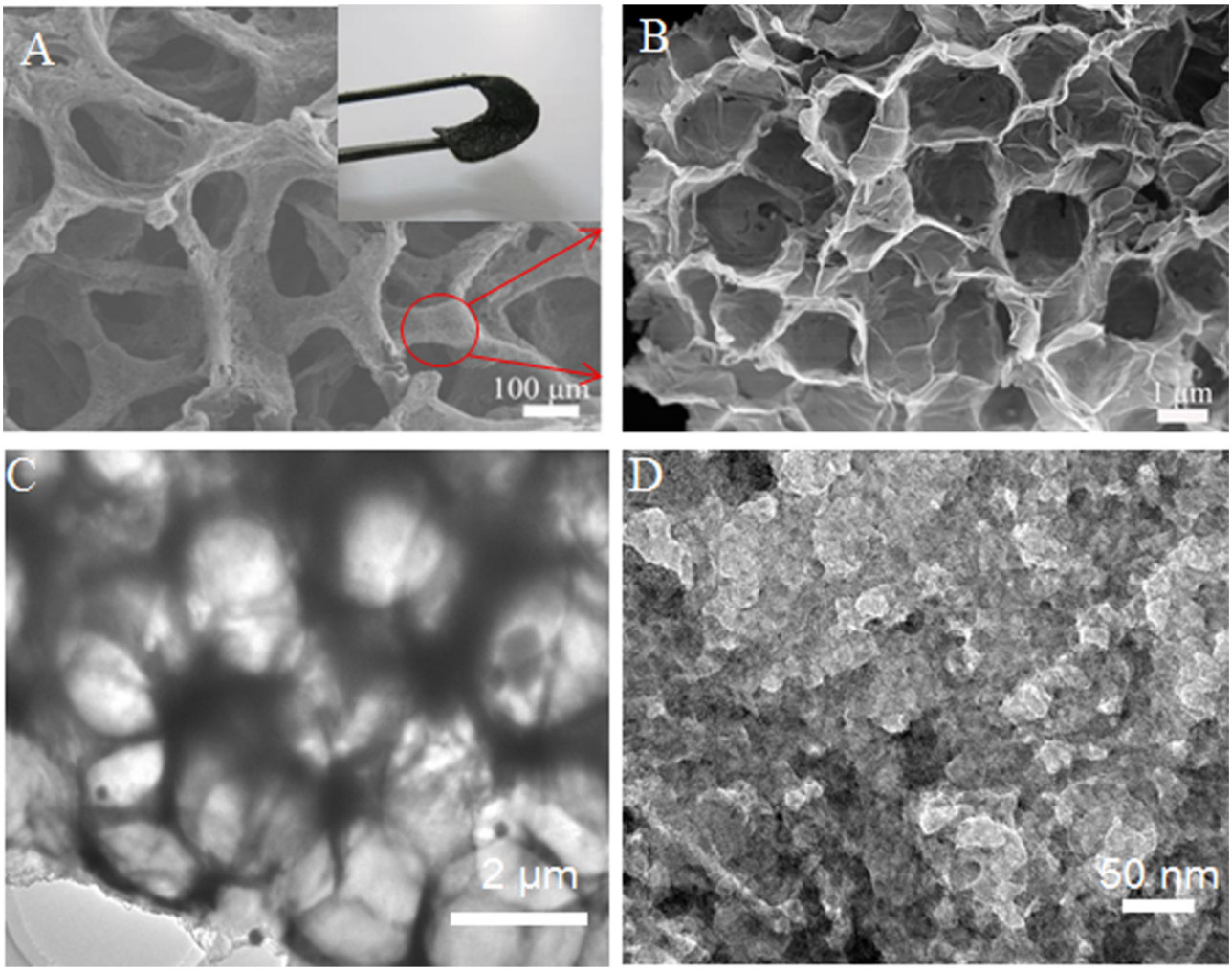

Fig. 2. SEM images (A and B) and TEM image(C and D) of fRGO-F at different magnifications. Inset in (A) is the fRGO-F digital graph.

components centred at 398.1 eV, 399.6 eV and 401.0 eV, corresponding to pyridinica-N, pyrrolic-N and graphitic-N, respectively (Fig. S3A). With increasing the PANI mass loadings in the composites, the N content dramatically increases to 1.33 at% and 3.03 at% for fRGO-F/PANI5 and fRGO-F/PANI7, respectively. The N 1s spectra of fRGO-F/PANI5 (Fig. S3B) and fRGO-F/PANI7 (Fig. 4D) can be derived into three components, which are ascribed to the pyridinic (—N=, 398.5 eV), pyrrolic (—NH—, 400.0 eV) and quaternary nitrogen (—NH^+=, 401.3 eV) [29,30] suggesting the successful deposition of PANI nanowires on the structures of fRGO-F.

3.2. Electrochemical performances

The free-standing 3D fRGO-F/PANI hybrids have excellent conductivity (966–1000 S m^{-1}) and large surface areas with hierarchical macroporous structure, making them ideal electrodes for supercapacitors. The two electrodes and a separator were assembled with 1 M H_2SO_4 as the electrolyte, and then encapsulated by a flexible poly (ethylene terephthalate) film. All the electrochemical performances of the as-prepared flexible supercapacitors were measured in a two-electrode system. Fig. 5A compares the CV curves of fRGO-F and RGO-F at the same scan rate of 10 mV s^{-1}. The fRGO-F device shows a larger current indicating its larger specific capacitance than that of RGO-F. The nearly symmetric CV curves for fRGO-F device at a scan rate ranging from 10 to 200 mV s^{-1} exhibit characteristic behaviour of electrical double layer capacitor, as shown in Fig. 5B. The novel hierarchically macro/mesoporous structures of fRGO-F electrode can enhance ion transport and also provide sufficient contact area between the electrode and electrolyte, which act as a skeleton network for the growth of PANI nanowires.

Fig. 6A shows the CV curves of fRGO-F, fRGO-F/PANI5 and fRGO-F/PANI7 supercapacitors at a scan rate of 10 mV s^{-1} in 1 M H_2SO_4. Compared with the curve of fRGO-F, the fRGO-F/PANI5 and fRGO-F/PANI7 show a higher current value and larger integrated area, suggesting the enhanced electrochemical capability by the incorporation of PANI nanowires on the 3D hierarchical porous graphene foams. Two pairs of redox peaks in the CV curves of fRGO-F/PANI5 and fRGO-F/PANI7 are attributed to the redox transition of leucoemeraldine/emeraldine and emeraldine/pernigraniline states of PANI [31]. The PANI nanowires deposited on the interface and surface of porous graphene can increase the specific surface area and provide more charge transfer pathways. The good capacitive feature is also confirmed by the galvanostatic charge/discharge curves at a current density of 1 A g^{-1} in Fig. 6B. Apparently, the curves of fRGO-F/PANI are almost symmetric, indicating high columbic efficiency because of the highly reversible redox reactions of PANI. The slight IR drop of fRGO-F/PANI5 (0.02 V) and fRGO-F/PANI7 (0.05 V) confirms that the devices has a small internal resistance, also further demonstrating that the PANI nanowires intimately anchored on the porous graphene surface can promote the transport and collection of electrons. Furthermore, the fRGO-F/PANI7 supercapacitor

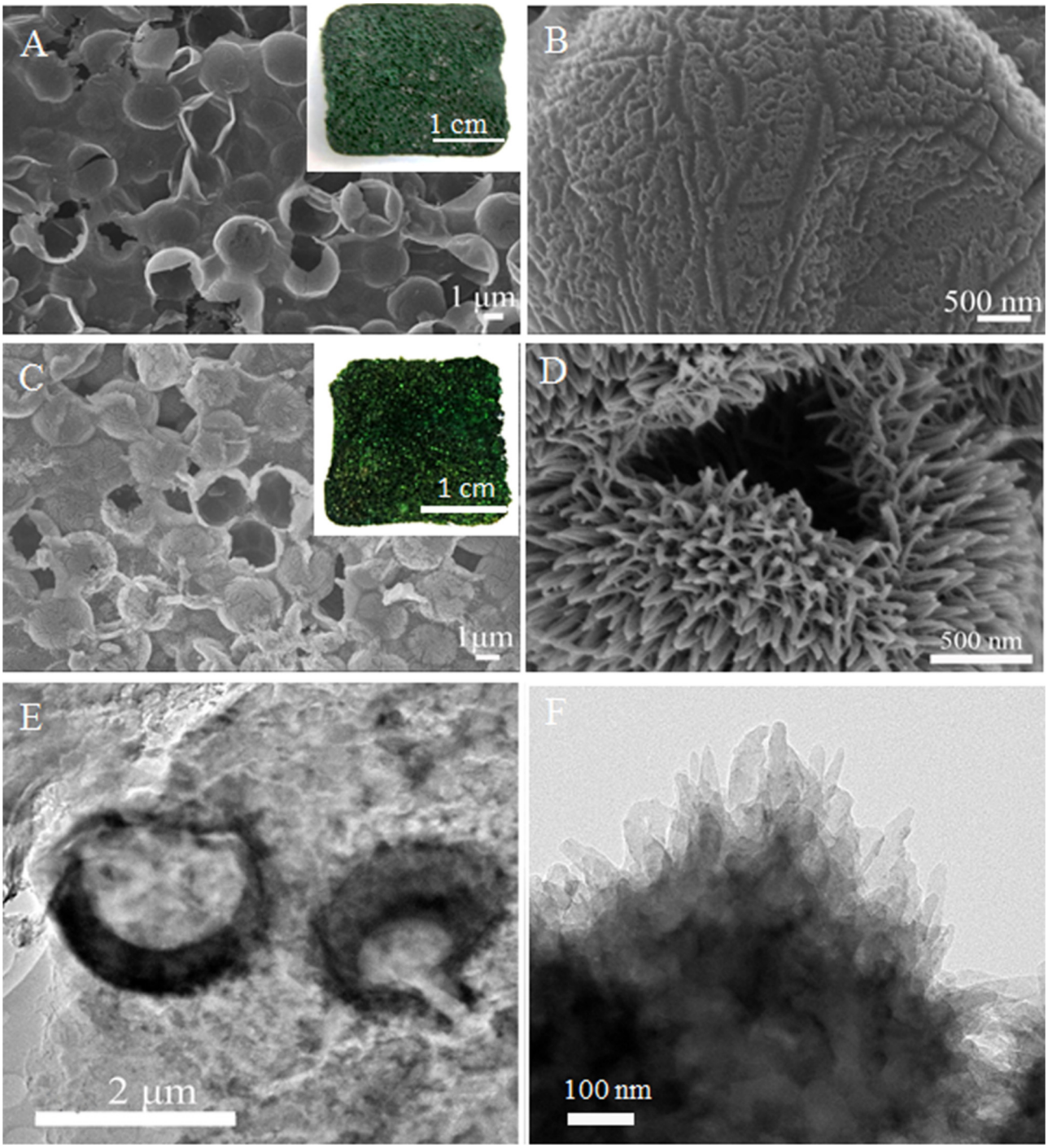

Fig. 3. SEM images (A and B) of fRGO-F/PANI5, and SEM images (C and D) and TEM images (E and F) of fRGO-F/PANI7 at low and high magnifications. Insets in (A,C) are their digital graphs.

shows good rate ability from both CV lines and charge/discharge curves at different scan rates and various current densities, respectively, as shown in Fig. 6C and D. It indicates that the 3D hierarchical macro/mesoporous structure is favourable for the effective ion migration into the interior surfaces, thus leading to the reversible capacitive behavior even at high scan rates.

The gravimetric specific capacitance of the three supercapacitors at various current densities was calculated from the discharge time (experimental sections), as shown in Fig. 7A. The specific capacitance of fRGO-F (145 F g^{-1}) is higher than some reported materials, such as RGO-F (100 F g^{-1}) [24] and porous graphene (79–93 F g^{-1}) [32,33], and is comparable to that of porous RGO-CNT on carbon cloth (151 F g^{-1}) [34]. Obviously, fRGO-F/PANI7 has a higher specific capacitance (939 F g^{-1}) than that of fRGO-F/PANI5 (895 F g^{-1}) and RGO-F/PANI5 (715 F g^{-1}) in our previous work [24], which is owing to the unique hierarchical macro/mesoporous structure and highly ordered PANI nanowires in the hybrid. Even at a high current density of 8 A g^{-1}, the specific capacitance of fRGO-F/PANI7 (803 F g^{-1}) is higher than RGO/PANI (257–763 F g^{-1}) [19,27,35,36], porous carbon/PANI (478–803 F g^{-1}) [37,38] and PS/RGO/PANI (180–682F g^{-1}) [22,29,39]. The thickness of fRGO-F and fRGO-F/PANI electrodes were 58, 60 and

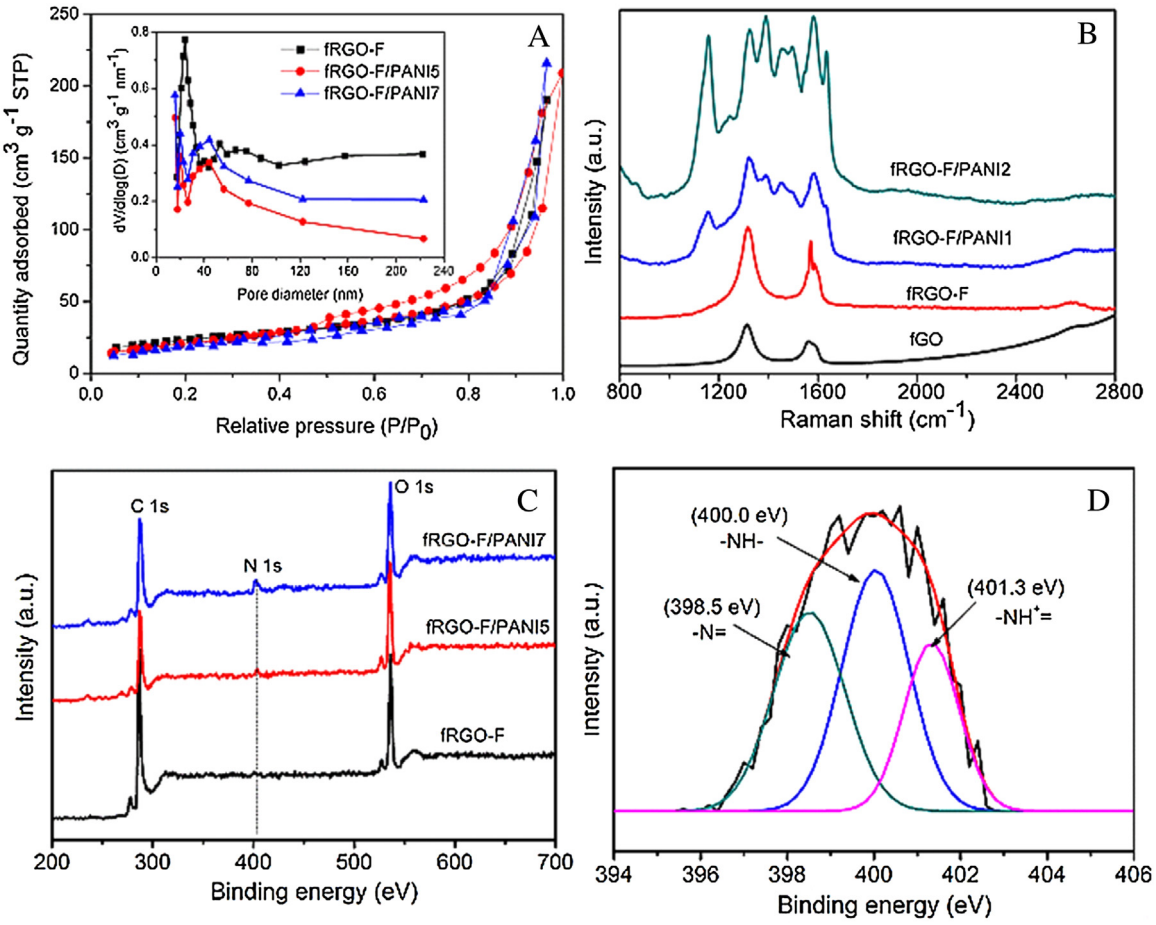

Fig. 4. (A) Nitrogen adsorption isotherms and pore size distributions (inset) of fRGO-F and fRGO-F/PANI composites. (B) Raman spectra of fGO, fRGO-F, fRGO-F/PANI5 and fRGO-F/PANI7 composites. (C) XPS spectra of fRGO-F, fRGO-F/PANI5 and fRGO-F/PANI7. (D) The high-resolution N 1s peak of fRGO-F/PANI7.

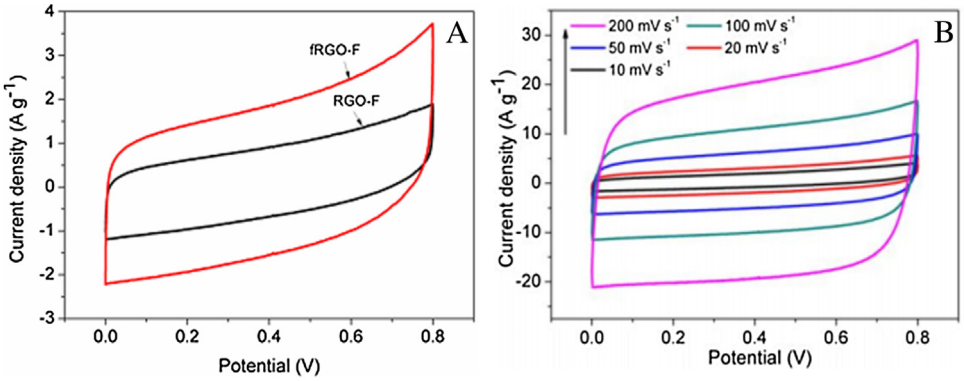

Fig. 5. (A) Comparison of CV curves of fRGO-F and RGO-F device at a scan rate of 10 mV s^{-1}. (B) CV curves of fRGO-F at various scan rates in 1 M H_2SO_4 solution.

63 ± 2 μm with a 15 MPa force applied, measured three times using the vernier caliper. Thus, the volumetric capacitance (C_{vol}) of fRGO-F/PANI5 and fRGO-F/PANI7 sample was calculated to be 232.7 ± 8 F cm^{-3} and 244.1 ± 8 F cm^{-3}, which is higher than RGO-F/PANI (205.4 F cm^{-3}) and carbide-derived carbon [40]. In the wide range of current densities, the fRGO-F, fRGO-F/PANI5 and fRGO-F/PANI7 could maintain a high retention efficiency of 86.2%, 75.8% and 85.5%, respectively. The porous graphene sheets connected with the opened hollow carbon spheres can form into conductive network and serve as a support of PANI, which maximized the exposed surface area to the electrolytes and minimized the diffusional losses in the high rate process to improve the rate capability.

EIS is an important tool for the study of the ion diffusion in the hierarchical porous structures. Fig. 7B shows the Nyquist plots of fRGO-F, fRGO-F/PANI5 and fRGO-F/PANI7 in the frequency range of 0.01–10^5 Hz at the open circuit potential with expanded plots in the inset. The equivalent circuit models of all supercapacitors are shown in Fig. S4, including the series resistance R_s, the pseudocapacitive capacitance C_L, the charge transfer resistance R_{ct}, the Warburg diffusion element W_O and the constant phase element (CPE) [41,42]. The Nyquist plot of fRGO-F is similar to that of fRGO-F/PANI, but showing a smaller semicircle in the high-frequency region followed by an almost vertical line at the low-frequency region, which reveals a good capacitive behaviour.

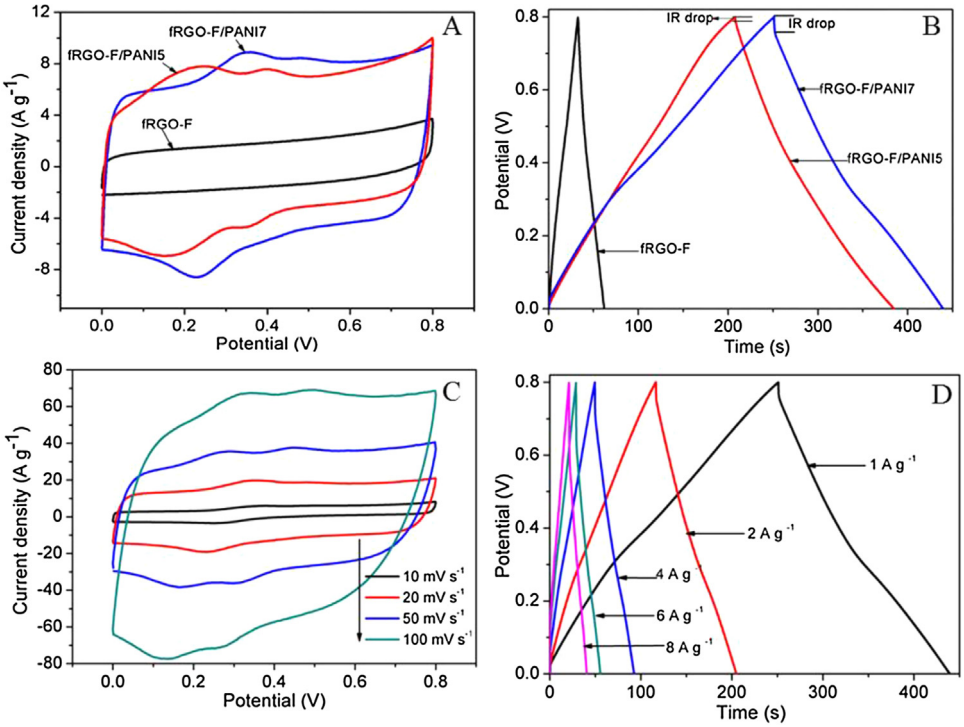

Fig. 6. (A) Cyclic voltammograms at a scan rate of 10 mV s^{-1} and (B) charge/discharge curves at 1 A g^{-1} for fRGO-F, fRGO-F/PANI5 and fRGO-F/PANI7. CV (C) and charge/discharge curves (D) with different rates for fRGO-F/PANI7 supercapacitor.

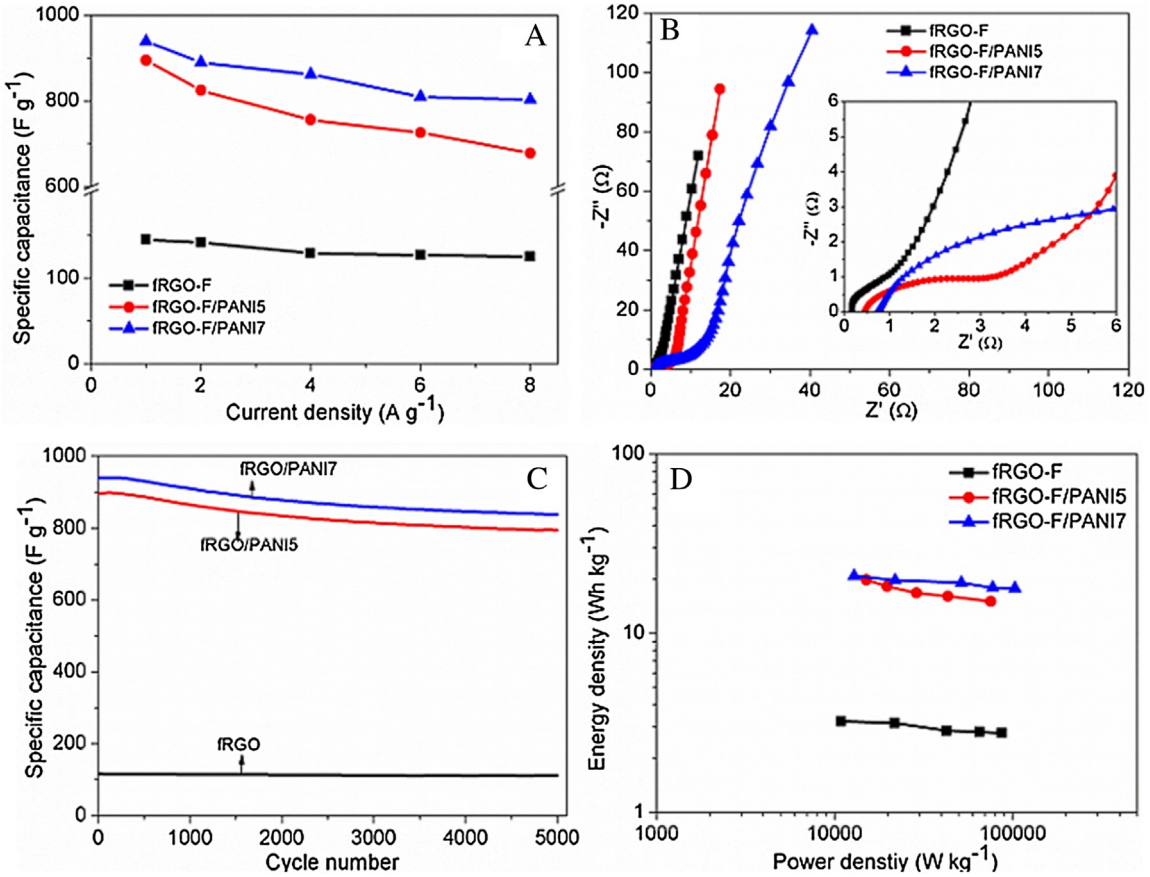

Fig. 7. Electrochemical performances of flexible supercapacitors based on fRGO-F, fRGO-F/PANI5 and fRGO-F/PANI7. (A) Gravimetric specific capacitance as a function of the current densities. (B) Nyquist plot at the frequency ranging from 0.01 to 10^5 Hz. (C) The cyclic stability at a constant current density of 1 A g^{-1} over 5000 cycles. (D) Ragone plot of energy density versus power density.

In the high-frequency, the semicircle suggests the porous network structure and the thickness of active materials [43]. The devices with fRGO-F/PANI as electrodes show relatively small equivalent series resistance (Rs) values (0.4–0.7 Ω) (Table S1), indicating lower internal resistance of the devices. The 3D flexible fRGO-F/PANI with a straight line in the low-frequency range correspond to an ideal capacitor and the capability of fast ion diffusion even with a high loading of PANI nanowires deposited on the hierarchical porous graphene foam.

The stability of the fRGO-F and fRGO-F/PANI supercapacitors was also evaluated by consecutive charge/discharge cycles at a current density of 1 A g^{-1} in Fig. 7C. The fRGO-F shows a good cyclic stability and keeps 96% of its initial capacitance after 5000 cycles. The fRGO-F/PANI5 and fRGO-F/PANI7 retain 89.3% and 88.7% of their initial values, which is higher than that of RGO/PANI5 (80%), respectively. The improvement results from the robust hierarchical porous support of the PANI nanowires on the internal surface of fRGO-F, making the electrode materials to be sufficiently exposed through the charge/discharge process. The specific capacitance of fRGO-F/PANI devices decrease gently in the first 1500 cycles and then almost stable until 5000 cycles. PANI nanowires as active materials of supercapacitors often suffer from poor cyclic stability due to the swelling, shrinkage and over oxidation of PANI nanowires during the charge/discharge processes. The interconnected hierarchical porous graphene networks can ensure the PANI nanowires deposit at nanoscale level on their surfaces with good interfacial contact, which enhances the restraint of destruction in the nanostructure during the H^+ insertion/extraction of the PANI [44]. The fRGO-F/PANI supercapacitors show an enhanced cyclic stability over the pure PANI (Fig. S5) due to the synergistic effects between PANI and fRGO-F. The optimal balance of active PANI nanowires in the hybrid electrodes and short transport distance, also together with strong π-π interactions between graphene spheres and PANI nanowires may synergistically contribute to the enhanced electrochemical performances. Moreover, the Nyquist plots of the fRGO-F and fRGO-F/PANI supercapacitors after 5000th cycles are presented in Fig. S6. The R_{ct} increased slightly from 1.6, 3.6 and 11.7 Ω to 2.1, 20 and 51 Ω for fRGO-F, fRGO-F/PANI5 and fRGO-F/PANI7, which suggesting that the nanostructures are well maintained and preserved overall with little structural deformation after long cycles. In addition, the increased Warburg resistance after 5000th cycles results from the detached active materials blocking the diffusion pathways.

The Ragone plots demonstrating the relationship between the energy and power density of the fRGO-Fand fRGO-F/PANI devices are shown in Fig. 7D. The energy density of fRGO-F supercapacitor is 3.2 Wh kg^{-1} at a power density of 11 kW kg^{-1} (1 A g^{-1}) and reduces slightly as the power density increases, which is higher than those of RGO-F (2.2 Wh kg^{-1}, 9.0 kW kg^{-1}) [31] and porous graphene/carbon cloth (1.6 Wh kg^{-1}, 0.7 kW kg^{-1}) [32]. It can be seen that the maximum energy density of 20.9 Wh kg^{-1} for the symmetric fRGO-F/PANI7 supercapacitor at a power density of 7.2 kW kg^{-1} can be achieved with the operating potential of 0.8 V. Moreover, the energy density of 17.8 Wh kg^{-1} can be kept at a power density of 103.2 kW kg^{-1}. These values are higher than those of fRGO-F, fRGO-F/PANI5 supercapacitors, and other devices reported previously including graphene/PANI (7.6 Wh kg^{-1}, 3.1 kW kg^{-1}) [19], RGO-F/PANI (17.6 Wh kg^{-1}, 98 kW kg^{-1}) [24], hierarchical porous carbon/PANI (18.5 Wh kg^{-1}, 0.1 kW kg^{-1}) [37], mesoporous graphene/PANI (11.3 Wh kg^{-1}, 0.1 kW kg^{-1}) [45], suggesting its good potential as freestanding electrodes for supercapacitors. Finally, the flexibility of the assembled fRGO-F/PANI7 device is further examined under the bending conditions. Fig. 8 shows the CV curves of fRGO-F/PANI7 device exhibit no significant change before and after bending (about 180°, inset images of Fig. 7), indicating excellent flexibility of freestanding hierarchical porous fRGO-F/PANI7 used as a flexible power source.

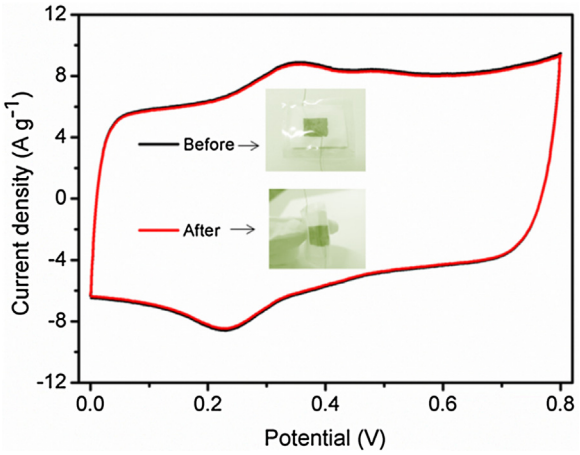

Fig. 8. CV curves at a scan rate of 10 mV s^{-1} and digital photograph of the fRGO/PANI7 device before and after bending.

4. Conclusions

In summary, the synergistic effects of hierarchical macro/mesoporous structure and PANI nanowires deposited on the graphene foam has been clearly demonstrated with high specific capacitance and cyclic stability flexible supercapacitor by a facile *in situ* polymerization. The 3D fRGO-F inherits uniform and controllable porous structures, providing rapid pathways for ionic and electronic transport to high specific capacitance. In particular, fRGO-F/PANI7 prepared by deposition of vertically aligned PANI nanowires onto porous graphene foam showed a 6-fold higher specific capacitance than that of fRGO-F. The symmetric fRGO-F/PANI7 supercapacitor exhibited a maximum energy density and power density of 20.9 Wh kg^{-1} and 103.2 kW kg^{-1}, respectively. It also achieves an excellent cyclic stability with 88.7% retention capacitance after 5000 cycles, attributing to the synergistic function of 3D hierarchical porous structure and effective PANI immobilization. Therefore, the interconnected hierarchical macro/mesoporous flexible graphene and PANI foam supercapacitor is a great potential to improve the electrochemical performance of energy storage systems.

Acknowledgements

This work was financially supported by the National Natural Science foundation of China (51403036), Shanghai Education Commission "Yangfan" Program (14YF1405300), Shanghai Education development foundation "Chenguang" Program (14S10656), Specialized Research Fund for the Doctoral Program of Higher Education of China (SRFDP 20130075120018), Fundamental Research Funds for the Central University (2232014D3-09) and Postdoctoral Science Foundation of China (2015M571487).

Appendix A. Supplementary data

Supplementary data associated with this article can be found, in the online version, at http://dx.doi.org/10.1016/j.apsusc.2016.09.119.

References

[1] L.L. Zhang, X.S. Zhao, Carbon-based materials as supercapacitor electrodes, Chem. Soc. Rev. 38 (2009) 2520–2531.

[2] S. Mao, Z. Wen, H. Kim, G. Lu, P. Hurley, J. Chen, A general approach to one-pot fabrication of crumpled graphene-based nanohybrids for energy applications, ACS Nano 6 (2012) 7505–7513.
[3] Z. Wen, X. Wang, S. Mao, Z. Bo, H. Kim, S. Cui, G. Lu, X. Feng, J. Chen, Crumpled nitrogen-doped graphene nanosheets with ultrahigh pore volume for high-performance supercapacitor, Adv. Mater. 24 (2012) 5610–5616.
[4] Z. Chen, W. Ren, L. Gao, B. Liu, S. Pei, H.M. Cheng, Three-dimensional flexible and conductive interconnected graphene networks grown by chemical vapour deposition, Nat. Mater. 10 (2011) 424–428.
[5] Y. He, W. Chen, X. Li, Z. Zhang, J. Fu, C. Zhao, E. Xie, Freestanding three-dimensional graphene/MnO_2 composite networks as ultralight and flexible supercapacitor electrodes, ACS Nano 7 (2012) 174–182.
[6] L. Jiang, Z. Fan, Design of advanced porous graphene materials: from graphene nanomesh to 3D architectures, Nanoscale 6 (2014) 1922–1945.
[7] Z.P. Chen, C. Xu, C.Q. Ma, W.C. Ren, H.M. Cheng, Lightweight and flexible graphene foam composites for high-performance electromagnetic interference shielding, Adv. Mater. 25 (2013) 1296–1300.
[8] N. Chen, Q. Pan, Versatile fabrication of ultralight magnetic foams and application for oil-water separation, ACS Nano 7 (2013) 6875–6883.
[9] A. Chen, P. Holt-Hindle, Platinum-based nanostructured materials: synthesis, properties, and applications, Chem. Rev. 110 (2010) 3767–3804.
[10] Z.S. Wu, Y. Sun, Y.Z. Tan, S. Yang, X. Feng, K. Mullen, Three-dimensional graphene-based macro- and mesoporous frameworks for high-performance electrochemical capacitive energy storage, J. Am. Chem. Soc. 134 (2012) 19532–19535.
[11] B.G. Choi, M. Yang, W.H. Hong, J.W. Choi, Y.S. Huh, 3D macroporous graphene frameworks for supercapacitors with high energy and power densities, ACS Nano 6 (2012) 4020–4028.
[12] X. Liu, Y. Wu, Z. Yang, F. Pan, X. Zhong, J. Wang, et al., Nitrogen-doped 3D macroporous graphene frameworks as anode for high performance lithium-ion batteries, J. Power Sources 293 (2015) 799–805.
[13] Z.L. Wang, D. Xu, H.G. Wang, Z. Wu, X.B. Zhang, In situ fabrication of porous graphene electrodes for high-performance energy storage, ACS Nano 7 (2013) 2422–2430.
[14] H. Qiu, X. Han, F. Qiu, J. Yang, Facile route to covalently-jointed graphene/polyaniline composite and it's enhanced electrochemical performances for supercapacitors, Appl. Surf. Sci. 376 (2016) 261–268.
[15] C. Yang, L. Zhang, N. Hu, Z. Yang, H. Wei, Z.J. Xu, Y. Wang, Y. Zhang, Densely-packed graphene/conducting polymer nanoparticle papers for high-volumetric-performance flexible all-solid-state supercapacitors, Appl. Surf. Sci. 379 (2016) 206–212.
[16] M. Naseri, L. Fotouhi, A. Ehsani, F. Babaei, Physicoelectrochemical properties of facilely electrosynthesized reduced graphene oxide/p-type conductive polymer nanocomposite film, New J. Chem. 40 (2016) 2565–2573.
[17] K. Wang, J.Y. Huang, Z. Wei, Conducting polyaniline nanowire arrays for high performance supercapacitors, J. Phys. Chem. C 114 (2010) 8062–8067.
[18] S. He, X. Hu, S. Chen, H.H. Hanif, H. Hou, Needle-like polyaniline nanowires on graphite nanofibers hierarchical micro/nano-architecture for high performance supercapacitors, J. Mater. Chem. 22 (2012) 5114–5120.
[19] L. Li, A.R. Raji, H. Fei, Y. Yang, E.L. Samuel, J.M. Tour, Nanocomposite of polyaniline nanorods grown on graphene nanoribbons for highly capacitive pseudocapacitors, ACS Appl. Mater. Interfaces 5 (2013) 6622–6627.
[20] G. Ćirić-Marjanović, Recent advances in polyaniline research: polymerization mechanisms, structural aspects, properties and applications, Synth. Met. 177 (2013) 1–47.
[21] S. Wang, L. Ma, M. Gan, S. Fu, W. Dai, T. Zhou, X. Sun, H. Wang, H. Wang, Free-standing 3D graphene/polyaniline composite film electrodes for high-performance supercapacitors, J. Power Sources 299 (2015) 347–355.
[22] J. Mu, C. Hou, H. Wang, Y. Li, Q. Zhang, Graphene-carbon nanotube papers for energy conversion and storage under sunlight and heat, Carbon 95 (2015) 150–156.
[23] J. Chen, Y. Liu, W. Li, C. Wu, L. Xu, H. Yang, Nanostructured polystyrene/polyaniline/graphene hybrid materials for electrochemical supercapacitor and Na-ion battery applications, J. Mater. Sci. 50 (2015) 5466–5474.
[24] P. Yu, X. Zhao, Z. Huang, Y. Li, Q. Zhang, Free-standing three-dimensional graphene and polyaniline nanowire arrays hybrid foams for high-performance flexible and lightweight supercapacitors, J. Mater. Chem. A 2 (2014) 14413–14420.
[25] X. Zhao, Q. Zhang, D. Chen, P. Lu, Enhanced mechanical properties of graphene-based poly(vinyl alcohol) composites, Macromolecules 43 (2010) 2357–2363.
[26] F. Jiang, W. Li, R. Zou, Q. Liu, K. Xu, L. An, J. Hu, MoO_3/PANI coaxial heterostructure nanobelts by in situ polymerization for high performance supercapacitors, Nano Energy 7 (2014) 72–79.
[27] S.H. Park, S.M. Bak, K.H. Kim, J.P. Jegal, S.I. Lee, J. Lee, K.B. Kim, Solid-state microwave irradiation synthesis of high quality graphene nanosheets under hydrogen containing atmosphere, J. Mater. Chem. 21 (2011) 680.
[28] D. Xu, Q. Xu, K. Wang, J. Chen, Z. Chen, Fabrication of free-standing hierarchical carbon nanofiber/graphene oxide/polyaniline films for supercapacitors, ACS Appl. Mater. Interfaces 6 (2014) 200–209.
[29] X. Ning, W. Zhong, S. Li, Y. Wang, W. Yang, High performance nitrogen-doped porous graphene/carbon frameworks for supercapacitors, J. Mater. Chem. A 2 (2014) 8859–8867.
[30] X. Liu, N. Wen, X. Wang, Y. Zheng, A high-performance hierarchical graphene@polyaniline@graphene sandwich containing hollow structures for supercapacitor electrodes, ACS Sustain. Chem. Eng. 3 (2015) 475–482.
[31] L. Zhang, L. Chen, B. Qi, G. Yang, J. Gong, Synthesis of vertical aligned TiO_2@polyaniline core-shell nanorods for high performance supercapacitors, RSC Adv. 5 (2015) 1680–1683.
[32] S.Y. Wang, B. Pei, X.S. Zhao, R.A.W. Dryfe, Highly porous graphene on carbon cloth as advanced electrodes for flexible all-solid-state supercapacitors, Nano Energy 2 (2013) 530–536.
[33] C.M. Chen, Q. Zhang, C.H. Huang, X.C. Zhao, B.S. Zhang, Q.Q. Kong, M.Z. Wang, Y.G. Yang, R. Cai, D. Sheng Su, Macroporous 'bubble' graphene film via template-directed ordered-assembly for high rate supercapacitors, Chem. Commun. 48 (2012) 7149–7151.
[34] S. Wang, R.A.W. Dryfe, Graphene oxide-assisted deposition of carbon nanotubes on carbon cloth as advanced binder-free electrodes for flexible supercapacitors, J. Mater. Chem. A 1 (2013) 5279.
[35] A. Ehsani, H. Mohammad Shiri, E. Kowsari, R. Safari, J. Torabian, S. Kazemi, Nanocomposite of p-type conductive polymer/functionalized graphene oxide nanosheets as novel and hybrid electrodes for highly capacitive pseudocapacitors, J. Colloid Interface Sci. 478 (2016) 181–187.
[36] J. Shabani Shayeh, A. Ehsani, M.R. Ganjali, P. Norouzi, B. Jaleh, Conductive polymer/reduced graphene oxide/Au nano particles as efficient composite materials in electrochemical supercapacitors, Appl. Surf. Sci. 353 (2015) 594–599.
[37] J. Hu, H. Wang, X. Huang, Improved electrochemical performance of hierarchical porous carbon/polyaniline composites, Electrochim. Acta 74 (2012) 98–104.
[38] Z. Lei, X. Sun, H. Wang, Z. Liu, X.S. Zhao, Platelet CMK-5 as an excellent mesoporous carbon to enhance the pseudocapacitance of polyaniline, ACS Appl. Mater. Interfaces 5 (2013) 7501–7508.
[39] W. Fan, Y.-E. Miao, L. Zhang, Y. Huang, T. Liu, Porous graphene?carbon nanotube hybrid paper as a flexible nano-scaffold for polyaniline immobilization and application in all-solid-state supercapacitors, RSC Adv. (2015) 31064–31073.
[40] D. Weingarth, D. Cericola, F.C.F. Mornaghini, T. Hucke, R. Kötz, Carbon additives for electrical double layer capacitor electrodes, J. Power Sources 266 (2014) 475–480.
[41] H.M. Shiri, A. Ehsani, J.S. Shayeh, Synthesis and highly efficient supercapacitorbehavior of a novel poly pyrrole/ceramic oxide nanocomposite film, RSC Adv. 5 (2015) 91062–91068.
[42] J. Torabian, M.G. Mahjani, H.M. Shiri, A. Ehsani, J.S. Shayeh, Facile electrosynthesis, characterisation and electrochemical performance of poly ortho aminophenol/$Al_5Y_3O_{12}$ nanocomposite as a new high efficient supercapacitor, RSC Adv. 6 (2016) 41045–41052.
[43] P.P. Yu, Y.Z. Li, X. Zhao, L.H. Wu, Q.H. Zhang, In situ growth of ordered polyaniline nanowires on surfactant stabilized exfoliated graphene as high-performance supercapacitor electrodes, Synth. Met. 185 (2013) 89–95.
[44] Y. Li, Q. Zhang, X. Zhao, P. Yu, L. Wu, D. Chen, Enhanced electrochemical performance of polyaniline/sulfonated polyhedral oligosilsesquioxane nanocomposites with porous and ordered hierarchical nanostructure, J. Mater. Chem. 22 (2012) 1884–1892.
[45] Q. Wang, J. Yan, Z. Fan, T. Wei, M. Zhang, X. Jing, Mesoporous polyaniline film on ultra-thin graphene sheets for high performance supercapacitors, J. Power Sources 247 (2014) 197–203.